DOI: 10.1002/adem.((please add manuscript number))

A multiscale approach for the non-linear mechanical response of 3-phases fiber reinforced graphene nanoplatelets polymer composite materials

By *Wiyao Azoti**, and *Ahmed Elmarakbi*

[*] *Dr. W. Azoti,*
ICUBE laboratory, CNRS UMR 7357, University of Strasbourg, 4 rue Boussingault, Strasbourg, 67000 France,
ECAM Strasbourg-Europe, School of Engineering, 2 rue de Madrid, Schiltigheim, 67300, France.
E-mail: ((wiyao.azoti@ecam-strasbourg.eu))
Prof. Dr. A. Elmarakbi
Automotive Composites, Department of Mechanical and Construction Engineering, Faculty of Engineering and Environment, Northumbria University, Newcastle NE1 8ST, UK.

Abstract

This work presents an analytical approach for solving the non-linear mechanical response of hybrid glass fibers reinforced graphene polymer composite materials. Two-scale homogenization technique derives the effective properties of the composite. At the first scale, the properties of a 2-phases graphene/polymer composite are obtained by accounting for the J2 plasticity coupled with the "Lemaitre-Chaboche" ductile damage model. An interfacial imperfection between the fillers and the matrix is considered through the linear spring model LSM. At the second scale, the modeling of the 3-phases glass fibers/graphene/polymer composite combines the 2-phases composite as a matrix phase in which are embedded the glass fibers. For both scales, a modified Mori-Tanaka scheme derives the effective properties. Numerical results, obtained for a thermoplastic PA6 matrix, are compared with the multistep method of Digimat software. Finally, a tension-torsion test shows that the imperfection of fibers/polymer interface is the driven parameter to weaken the mechanical responses in the shear direction.

Keywords: *graphene nanoplatelets, micromechanics, interface, ductile damage, 3-phases composite*

1. Introduction

Fibers reinforced polymer composite materials FRPCMs are well acknowledged for lightweighting due to their outstanding mechanical properties and high strength to weight ratio. However, FRPCMs need to overcome certain drawbacks related to poor transverse mechanical properties [1] and an interfacial interaction problem [2, 3] leading to an ineffective stress transfer and easy crack initiation and propagation [4]. The solution for such limitations passes upon the development of new fillers that can preserve the composite interfacial properties. As a contribution for solving such limitations, graphene based nanocomposites have been widely used for enhancing the multifunctional properties of polymer composite materials [5-11]

Besides, the development of advanced hybrid graphene-based polymer composites constitutes an efficient way to replace conventional composites in structural applications. Indeed, hybrid glass fibers GF reinforced graphene nanoplatelets GNP polypropylene PP composites have shown that the combined effect of the two fillers of rather different size scales i.e. micro- and nanoscale can lead to significant improvement of the tensile modulus and impact strength [12, 13]. Moreover, the dispersion of the nanofiller in the PP matrix promoted the formation of a stronger interface between the matrix and GF. The carbon fibers CF and GNPs reinforced poly-arylene ether nitrile (PEN) PEN/CF/GNP composites have demonstrated the synergic effect of combining reinforcements to deliver excellent mechanical properties higher 1.7, 4.5 and 6.4 times larger than those of PEN/CF composites, PEN/GNP composites and PEN host, respectively [4]. Several experimental techniques investigate the mechanical and interfacial properties of the hybrid fibers/nanofillers/polymer composites [14-16]. However, few researches [17, 18] have been devoted to the modeling and simulation of the hybrid nanocomposites. Except works by Feng et al. [19, 20] on the reorientation of graphene platelets on the mechanical properties of polymer nanocomposites, there is a lack of analytical developments (at the authors' best knowledge) devoted to the multiscale modelling of the hybrid nanocomposites to support simulations for structural applications.

In this work, an algorithm based on a multiscale modelling is proposed for deriving the hierarchical mechanical properties of the hybrid fibers reinforced graphene polymer matrix composites FRGPMCs. Multiscale modeling represents a powerful tool for dealing with the effective properties of composite materials. Boehm [21] proposes a good review of the multiscale modeling based on micromechanics approaches. Herein, the graphene is considered as continuum platelets embedded within a rate-independent elasto-plastic polymer matrix. For the nonlinear matrix, Lemaitre and Chaboche's model introduces a ductile damage behavior within the composite. A linear spring model LSM studies the interface between the reinforcements and the matrix. As a homogenization scheme, a modified Mori-Tanaka scheme derives the effective non-linear response of the 2-phases composite. Next, the fibers are embedded within the 2-phases composite leading to the 3-phases composite. Numerical results show that the volume fraction and the interfacial sliding coefficient have an influence on the effective nonlinear stress-strain behavior. It is shown through a tension-torsion loading that the fibers/polymer interface is the parameter to damage the composite mainly under a shear loading.

2. Micromechanics formulation

2.1. Effective properties based on the LSM model

Let us consider a macroscopic homogeneous and microscopic heterogeneous material under the assumption of a representative volume element RVE. The associated boundary-value problems are formulated, in the terms of uniform macro field traction vector or linear displacement fields with body forces and inertia term neglected. The effective properties are given by:

$$C_{ijkl}^{eff} = \frac{1}{V}\int_{V} c_{ijmn}(r)\, A_{mnkl}(r) dV \qquad (1)$$

Or in others terms

$$\boldsymbol{C}^{eff} = \sum_{I=0}^{N} f_I \boldsymbol{c}^I : \boldsymbol{A}^I \tag{2}$$

with $\boldsymbol{c}^I$, $\boldsymbol{A}^I$, f_I the uniform stiffness tensor, the global strain concentration tensor and the volume fraction of phase I respectively. By considering the interface between two phases of a composite material, the linear spring model LSM supposes the continuity of the traction vector across the interface while the jump of displacement field is considered to be proportional to the traction on that interface. Based on these assumptions, the modified Mori-Tanaka effective properties for multiphasic composite are given such as [22-24]:

$$\begin{cases} \mathbf{C}_{\mathrm{modified}}^{MT} = \left(f_0 \boldsymbol{c}^0 + \sum_{I=1}^{N} f_I \boldsymbol{c}^I : \boldsymbol{a}^I \right) \\ \qquad : \left[\sum_{I=0}^{N} f_I \boldsymbol{a}^I + \sum_{I=1}^{N} f_I \mathbf{H}^I : \boldsymbol{c}^I : \boldsymbol{a}^I \right]^{-1} \end{cases} \tag{3}$$

where $\boldsymbol{a}^I$ states for the local strain concentration tensor of the phase I. The relationship between the global $\boldsymbol{A}^I$ and local $\boldsymbol{a}^I$ strain concentration tensors yields:

$$\begin{cases} \boldsymbol{A}^I = \boldsymbol{a}^I : \mathbf{A}^0 \\ \boldsymbol{a}^I = \left[\mathbf{I} + \mathbf{S}^{\mathbf{M}} : \left(\boldsymbol{c}^0 \right)^{-1} : \Delta \boldsymbol{c}^I \right]^{-1} \\ \mathbf{A}^0 = \left[\sum_{I=0}^{N} f_I \boldsymbol{a}^I + \sum_{I=1}^{N} f_I \mathbf{H}^I : \boldsymbol{c}^I : \boldsymbol{a}^I \right]^{-1} \\ I = 1, 2, 3, ..., N \end{cases} \tag{4}$$

In Eq. (4), $\mathbf{S}^{\mathbf{M}}$ and $\mathbf{H}^I$ denote the modified Eshelby's tensor and a four-order tensor depending on the interface properties and the geometry of the inclusion, respectively. Expressions of $\mathbf{S}^{\mathbf{M}}$ and $\mathbf{H}^I$ for ellipsoidal inclusions can be found in works by Qu [25, 26]. The modified Eshelby's tensor for this problem yields:

$$\mathbf{S}^{\mathbf{M}} = \mathbf{S} + (\mathbf{I} - \mathbf{S}) : \mathbf{H} : \boldsymbol{c} : (\mathbf{I} - \mathbf{S}) \tag{5}$$

where $\mathbf{S}$ denotes the original Eshelby's tensor [27]. The components of the interfacial tensor $\mathbf{H}$ are given by:

$$H_{ijkl} = \alpha P_{ijkl} + (\beta - \alpha) Q_{ijkl} \tag{6}$$

where P_{ijkl} and Q_{ijkl} are given for ellipsoidal inclusions by:

$$\begin{cases} P_{ijkl} = \dfrac{3}{16\pi}\displaystyle\int_0^{\pi}\left[\int_0^{2\pi}\begin{pmatrix}\delta_{ik}n_j n_l + \delta_{jk}n_i n_l + \\ \delta_{il}n_k n_j + \delta_{jl}n_k n_i\end{pmatrix}\mathbf{n}^{-1}d\theta\right]\sin\phi d\phi \\ Q_{ijkl} = \dfrac{3}{4\pi}\displaystyle\int_0^{\pi}\left[\int_0^{2\pi}\left(n_i n_j n_k n_l\right)\mathbf{n}^{-3}d\theta\right]\sin\phi d\phi \\ \mathbf{n} = \sqrt{n_i n_i} \\ n = \left(\dfrac{\sin\phi\cos\theta}{a_1};\dfrac{\sin\phi\sin\theta}{a_2};\dfrac{\cos\phi}{a_3}\right)^{\mathrm{T}} \end{cases} \tag{7}$$

The constants α and β stand for the extent of interfacial sliding and the interfacial separation, respectively.

2.2 Ductile damage tangent modulus

The concept of the effective stress $\hat{\boldsymbol{\sigma}}$ describes the damage variable D ($0 \leq D < 1$). It characterizes the undamaged representation of the RVE. The effective stress is related to the damaged stress $\boldsymbol{\sigma}$ such as:

$$\hat{\boldsymbol{\sigma}} = \frac{\boldsymbol{\sigma}}{(1-D)} \tag{8}$$

Doghri and Ouaar [28] define at least two tangent operators for the non-linear stiffness: the effective elasto-plastic $\hat{\boldsymbol{C}}^{ep}$ tangent operator, which is derived from the rate constitutive equation, and the algorithmic $\boldsymbol{C}^{a\lg}$ (algorithmic effective $\hat{\boldsymbol{C}}^{a\lg}$) tangent operator, which is solved using a discretization in the time interval $[t_n, t_{n+1}]$. These tangent operators are related to the rate of the constitutive equation as follows:

$$\begin{cases} \dot{\hat{\boldsymbol{\sigma}}} = \hat{\boldsymbol{C}}^{ep} : \dot{\boldsymbol{\varepsilon}} \\ \delta\hat{\boldsymbol{\sigma}}_{n+1} = \hat{\boldsymbol{C}}^{a\lg} : \delta\boldsymbol{\varepsilon}_{n+1} \\ \delta\boldsymbol{\sigma}_{n+1} = \boldsymbol{C}^{a\lg} : \delta\boldsymbol{\varepsilon}_{n+1} \end{cases} \tag{9}$$

The above tangent operators are obtained from the classical J_2 plasticity and "Lemaitre-Chaboche" ductile damage model such as:

$$\begin{cases} \boldsymbol{\sigma} = (1-D)\boldsymbol{C}^{el} : \left(\boldsymbol{\varepsilon} - \boldsymbol{\varepsilon}^{p}\right) \\ f\left(\boldsymbol{\sigma}, R, D\right) = J_2\left(\hat{\boldsymbol{\sigma}}\right) - R\left(r\right) - \sigma_Y \\ J_2\left(\hat{\boldsymbol{\sigma}}\right) = \left[\frac{3}{2}\hat{\boldsymbol{s}} : \hat{\boldsymbol{s}}\right]^{1/2} \\ \hat{\boldsymbol{s}} = \hat{\boldsymbol{\sigma}} - \frac{1}{3} tr\hat{\boldsymbol{\sigma}}\mathbf{1} \\ \dot{\boldsymbol{\varepsilon}}^{p} = \dot{p}\hat{\boldsymbol{N}},\ \dot{p} = \left(\frac{2}{3}\dot{\boldsymbol{\varepsilon}}^{p} : \dot{\boldsymbol{\varepsilon}}^{p}\right)^{1/2} \\ \dot{r} = (1-D)\,\dot{p} \text{ with } \dot{r} \geq 0,\ \dot{r}f = 0,\ \dot{r}\dot{f} = 0 \\ \hat{\boldsymbol{N}} = \frac{\partial f}{\partial \hat{\boldsymbol{\sigma}}} = \frac{3}{2}\frac{\hat{\boldsymbol{s}}}{J_2\left(\hat{\boldsymbol{\sigma}}\right)} \\ \dot{D} = \left(\frac{Y}{S_0}\right)^{s} \dot{p} \text{ if } p \geq p_c \text{ and } D \leq D_c \end{cases} \tag{10}$$

The effective elasto-plastic $\hat{\boldsymbol{C}}^{ep}$ tangent operator yields:

$$\begin{cases} \hat{\boldsymbol{C}}^{ep} = \boldsymbol{C}^{el} - \frac{(2\mu)^2}{h}\hat{\boldsymbol{N}} \otimes \hat{\boldsymbol{N}} \\ h = 3\mu + \frac{dR}{dp} > 0 \end{cases} \tag{11}$$

while the effective algorithmic $\hat{\boldsymbol{C}}^{alg}$ tangent operator is given by:

$$\begin{cases} \hat{\boldsymbol{C}}^{alg} = \hat{\boldsymbol{C}}^{ep} - (2\mu)^2 \Delta p \frac{\hat{\sigma}_{eq}}{\hat{\sigma}_{eq}^{tr}} \frac{\partial \hat{\boldsymbol{N}}}{\partial \hat{\boldsymbol{\sigma}}} \\ \frac{\partial \hat{\boldsymbol{N}}}{\partial \hat{\boldsymbol{\sigma}}} = \frac{1}{\sigma_{eq}} \frac{3}{2} \mathbf{I}^{dev} - \hat{\boldsymbol{N}} \otimes \hat{\boldsymbol{N}} \end{cases} \tag{12}$$

In equations (11) and (12), μ denotes the material shear modulus while $\boldsymbol{C}^{el}$ represents the elastic stiffness tensor and $R(p)$ is the hardening stress function with p the accumulated plastic strain. $\boldsymbol{N}$ represents the normal to the yield surface in the stress space. σ_{eq}^{tr} denotes a trial elastic predictor of σ_{eq}. $\mathbf{I}^{dev}$ stands for the deviatoric part of the fourth order symmetric identity tensor. The internal variables such as Δp and σ_{eq}^{tr} are important for computing the algorithmic tangent operator in Eq. (12). Azoti et al. [29] present a detailed procedure about the update of internal variables.

$\boldsymbol{C}^{alg}$ will be later used to determine the effective behavior of the composite using the modified MT

scheme by Eqs. (3)-(7). From the Eq. (9) the algorithmic tangent operator $\boldsymbol{C}^{alg}$ can be obtained by:

$$\boldsymbol{C}^{alg} = (1-D)\hat{\boldsymbol{C}}^{alg} \tag{13}$$

3. Methods for the hierarchical modelling

3.1. Modelling strategy

The multiscale strategy shown by Figure 1 is set up around two points:

- The modelling of *2-phases graphene/polymer* composite. The mechanical properties of the graphene which are widely derived at the atomistic scale [30, 31] are considered through graphene platelets GNPs as continuum phases interacting with a rate-independent elasto plastic polymer matrix. The composite response is therefore computed under a boundary value problem by applying static or kinematic admissible loading. Mean-field homogenization schemes for instance the Mori-Tanaka are applied to obtain the overall response [22-24].
- The modelling of *3-phases fibres/graphene polymer* composite. It consists on a double-scale approach combining the *2-phases graphene/polymer* composite developed above as matrix phase in which are embedded the fibers. The derivation of the effective properties remains analytical-based formalism.

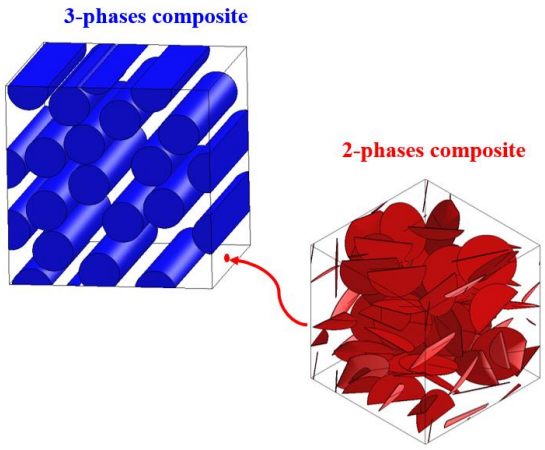

Figure1: Schematics of the multiscale modelling of the hybrid 3-phases composite.

3.2. Volume fraction management

Let us consider the 3-phases composite and let us denote $\varphi_F,\ \varphi_I,\ \varphi_0$ the volume fraction of the fibers, the GNPs and the polymer matrix respectively. They represent the input volume fractions of the problem. The total volume fraction φ_T is given such as:

$$\varphi_T = \varphi_F + \varphi_I + \varphi_0 = 1 \tag{14}$$

The volume fraction φ_{I0} of the 2-phases composite (GNPs/Polymer) considered as a matrix is given by:

$$\varphi_{I0} = \varphi_I + \varphi_0 = 1 - \varphi_T \tag{15}$$

Within the 2-phases composite (GNPs/Polymer), let us denote $f_I,\ f_0$ the volume fraction of GNPs and the polymer matrix respectively. These volume fractions yield:

$$\begin{cases} f_I = \dfrac{\varphi_I}{\varphi_{I0}} \\ f_0 = \dfrac{\varphi_0}{\varphi_{I0}} \\ f_I + f_0 = 1 \end{cases} \tag{16}$$

In summary, the effective properties of the 2-phases composite (GNPs/Polymer) are computed with $f_I,\ f_0$ while the effective properties of the 3-phases composite are computed with $\varphi_F,\ \varphi_I,\ \varphi_0$**.** These volume fractions will be used in the sequel for deriving the mechanical properties through a developed algorithm.

3.3. Algorithm for solving the effective properties

The input for the algorithm is the strain increment $\Delta\mathbf{E}$, which comes either analytically or numerically from Finite Element code. $\Delta\mathbf{E}$ is split between the phases of the 3-phases composite.Voigt assumption states the strain increment in the fibers while an averaged technique expresses the strain increment in the 2-phases Graphene/Polymer composite considered as a matrix.

Inside the 2-phases Graphene/Polymer composite, the strain increment is one more time switched between the Graphene inclusions and the Polymer matrix. Once the strain field is well equilibrated between the phases after a convergence check, the modified Mori-Tanaka scheme for imperfect interfaces computes the global strain concentration tensor and the effective properties of the 2-phases composite. At the next step, these effective properties for the 2-phases composite are used conjunctly with the algorithmic tangent modulus of the fibers to provide the whole 3-phases composite with the global strain concentration tensor and finally the effective tangent modulus through a convergence checking. The output of the algorithm is the stress increment $\Delta\sum$, which describes the multiscale modelling of the hybrid composite. The following steps summarize the constitutive algorithm presented in Figure 2.

1. Initialization of the strain increment in the fibers $\Delta\boldsymbol{\varepsilon}^F = \mathbf{A}^F : \Delta\mathbf{E}$ such as $\mathbf{A}^F = \mathbf{I}$

Update the stress in the fibers and compute the fibers algorithmic modulus $\boldsymbol{C}_F^{alg}$ using Eq.(13)

Apply the mid-point rule at time $t_{n+\alpha}$ to the algorithmic moduli of the fibers such as

$$\left[\boldsymbol{C}_F^{alg}\right]_{n+\alpha} = (1-\xi)\left[\boldsymbol{C}_F^{alg}\right]_n + \xi\left[\boldsymbol{C}_F^{alg}\right]_{n+1},\ \xi \in [0,1]$$

2. Compute the strain increment in the 2-phases composite $\Delta\boldsymbol{\varepsilon}^{I0} = \dfrac{\Delta\mathbf{E} - \varphi_F \Delta\boldsymbol{\varepsilon}^F}{1-\varphi_F}$

2.1. Initialization of the strain increment in the GNP $\Delta\boldsymbol{\varepsilon}^I = \mathbf{A}^I : \Delta\boldsymbol{\varepsilon}^{I0}$ such as $\mathbf{A}^I = \mathbf{I}$

Update the stress in the GNP and compute the GNP algorithmic modulus $\boldsymbol{C}_I^{alg}$ using Eq.(13)

Apply the mid-point rule at time $t_{n+\alpha}$ to the algorithmic modulus of the GNP such as

$$\left[\boldsymbol{C}_I^{alg}\right]_{n+\alpha} = (1-\xi)\left[\boldsymbol{C}_I^{alg}\right]_n + \xi\left[\boldsymbol{C}_I^{alg}\right]_{n+1},\ \xi \in [0,1]$$

2.2 Compute the strain increment in the polymer matrix $\Delta\boldsymbol{\varepsilon}^0 = \dfrac{\Delta\boldsymbol{\varepsilon}^{I0} - f_I \Delta\boldsymbol{\varepsilon}^I}{1-f_I}$

Update the stress in the matrix and compute the matrix algorithmic modulus $\boldsymbol{C}_0^{alg}$ using Eq.(13)

Apply the mid-point rule at time $t_{n+\alpha}$ to the algorithmic modulus of the matrix such as

$$\left[\boldsymbol{C}_0^{alg}\right]_{n+\alpha} = (1-\xi)\left[\boldsymbol{C}_0^{alg}\right]_n + \xi\left[\boldsymbol{C}_0^{alg}\right]_{n+1},\ \xi \in [0,1]$$

2.3 Compute the global strain concentration tensor of GNP such as $\boldsymbol{A}^I = \boldsymbol{a}^I : \mathbf{A}^0$ using Eq.(4)

2.4 Compute the residual $R = \boldsymbol{A}^I : \Delta\boldsymbol{\varepsilon}^{I0} - \Delta\boldsymbol{\varepsilon}^I$

2.5 If $|R| \le \text{TOL}=10^{-8}$, then exit the loop and go to step 2.7

2.6 Else, go to step 2.1 using the computed value of the global strain concentration tensor $\boldsymbol{A}^I$

2.7 Compute the effective tangent modulus $\mathbf{C}_{IO}^{eff}$ of the 2-phases composite using Eq.(3) along with the algorithmic moduli in steps 2.1 and 2.2

3. Using $\mathbf{C}_{IO}^{eff}$ as a matrix phase, compute global strain concentration tensor of the fibres such as $\boldsymbol{A}^F = \boldsymbol{a}^F : \mathbf{A}^{I0}$ using Eq.(4)

4. Compute the residual $R = \boldsymbol{A}^F : \Delta\mathbf{E} - \Delta\boldsymbol{\varepsilon}^F$

5 If $|R| \le \text{TOL}=10^{-8}$, then exit the loop and go to step 7

6. Else, go to step 1 using the computed value of the global strain concentration tensor of the fibres $\boldsymbol{A}^F$

7. Compute the effective tangent modulus $\mathbf{C}_{FIO}^{eff}$ of the 3-phases composite using Eq.(3) along with the algorithmic modulus in step 1 and the effective tangent modulus $\mathbf{C}_{IO}^{eff}$ in step 2.7

8. Finally, compute the macroscopic stress increment $\Delta\boldsymbol{\Sigma} = \mathbf{C}_{FIO}^{eff} : \Delta\mathbf{E}$

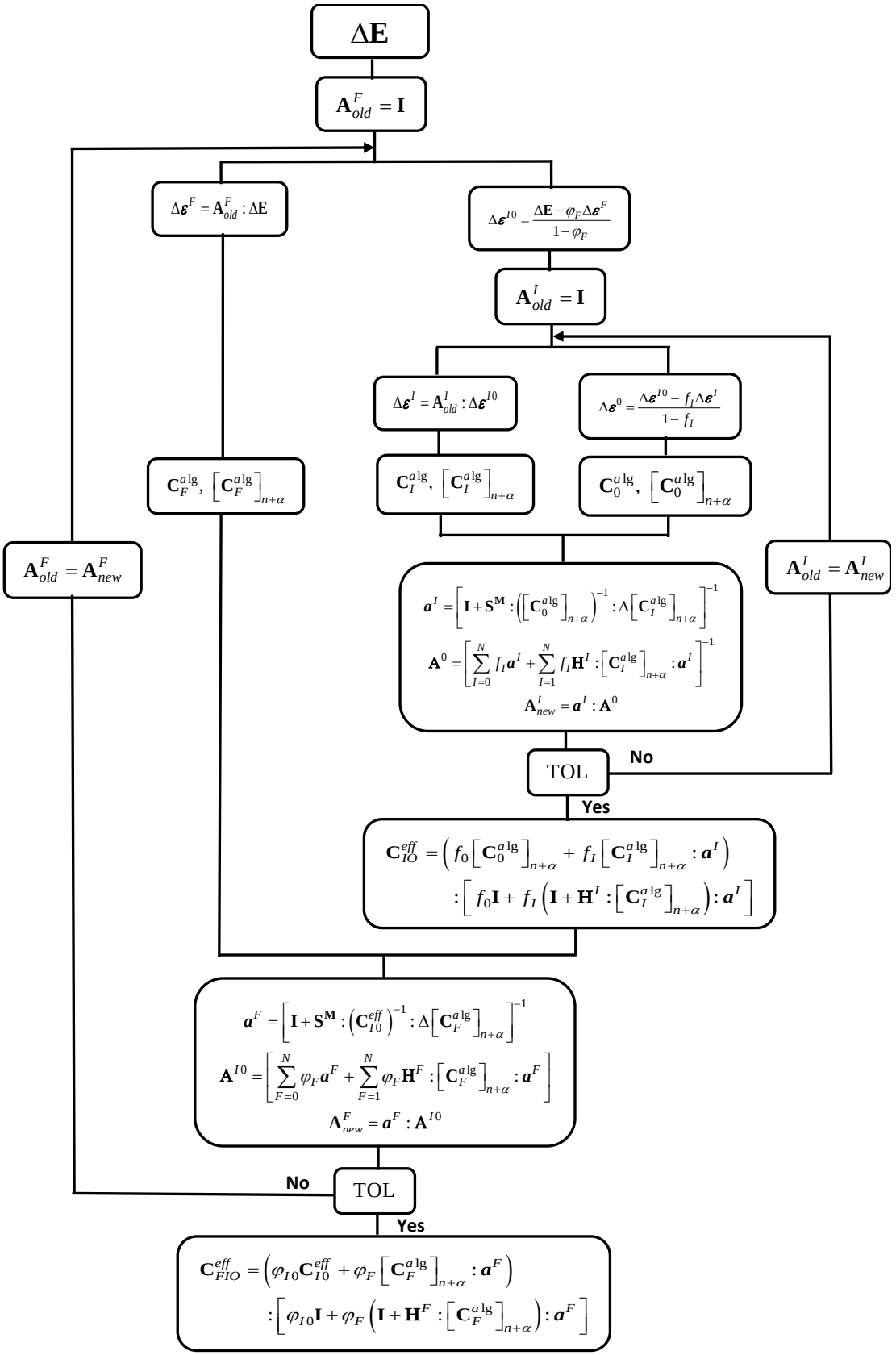

Figure2: Algorithm for solving the nonlinear response of the 3-phases composite

4. Results and discussions

Numerical results are conducted on a 3-phases composite. As the matrix phase, a thermoplastic PA6 polymer is used while graphene platelets GNPs and short E-Glass fibres are considered as reinforcements. In order to simulate the aspect ratio AR, ellipsoidal inclusions of dimensions (a_1, a_2, a_3) with aspect ratio AR such as $AR = a_3/a_1$ and $a_1 = a_2 = a$ are used for the homogenization. A pure sliding case is considered i.e $\alpha \neq 0$ and $\beta = 0$. The sliding interfacial separation constant α is given such as $\alpha = a\alpha_0/\mu_0$ with α_0 the sliding coefficient, a the ellipsoid semi-axis and μ_0 the shear modulus of the matrix. Since two interfaces are concerned in this work, it is denoted by α_{01} the sliding coefficient for the interface between the graphene nanoplatelets and the polymer matrix while α_{02} stands for the sliding coefficient of the interface between the short E-Glass fibers and the polymer matrix. Material properties used for the analysis are gathered in Table1 and Table 2. The aspect ratio of the GNPs and that of the short E-Glass fibers are given by Table 3.

Table 1: Material properties for the reinforcements

Short E-Glass fibers		Graphene G2NAN	
E_{EGF}	ν_{EGF}	E_I	ν_I
85 GPa	0.23	700 GPa	0.22

Table 2: Material properties for the polymer matrix

Matrix (Polymer PA6-B3K)						
E_0	ν_0	σ_Y	k	m	S^0	s
2000 MPa	0.39	60.5 MPa	63 MPa	0.4	2 MPa	0.5

Table 3: Aspect ratio AR for the reinforcements

Aspect Ratio AR	
Graphene platelets GNPs	Short E-Glass fibers
$AR = 10^{-3}$	$AR = 10$

The GPNs are assumed elastic while the PA-6 matrix is considered elasto-plastic with an isotropic hardening power law defined as $R(p) = kp^m$. The macro stress-strain response is studied under uniaxial loading. The loading is given by a macro stain increment such as $\Delta\mathbf{E} = \Delta E\, \boldsymbol{\psi}$ with $\boldsymbol{\psi} = \mathbf{e}_1 \otimes \mathbf{e}_1 - \frac{1}{2}[\mathbf{e}_2 \otimes \mathbf{e}_2 + \mathbf{e}_3 \otimes \mathbf{e}_3]$. The effective response of the composite is assessed through different design parameters for instance the platelets aspect ratio AR, the volume fraction f_I and the interface sliding coefficient α_{01}, α_{02} for both interfaces.

Figure 3 shows the evolution of the effective stress versus the equivalent strain for different volume fraction φ_F of short glass fibers. The analyses have been conducted for 2 sets of volume fraction φ_F mainly lower and moderate volume fractions. Figure 3.a-b addressed the studied volume fractions. In both cases, the effective behavior is enhanced with the increase of φ_F. The higher the volume fraction φ_F, the better the equivalent stress of the 3-phases composite material. The results are plotted along with the PA-6 matrix behavior. Present developments are compared with simulations performed with Digimat-MF [32]. Indeed, for low volume fraction φ_F, a fair agreement is found between the present model and Digimat. However, Digimat overestimates present modelling when φ_F increases. Indeed, the Mori-Tanaka scheme has been implemented for both scales i.e the 2-phases and 3-phases composites while Digimat employs the so-called "multi-step" procedure for dealing with the homogenization of composite materials, which contain more than 2 phases. The multi-step procedure therefore uses a different approach. A first step consists on the separation of the multiphasic composite into several domains of 2-phases composites that will be homogenized by the Mori-Tanaka scheme. A Voigt model is then used afterwards for the final

effective response of the multi-phasic composites. The present development and the "multi-step" procedure are quite different approaches. This fact is explaining the gap obtain for high volume fraction of φ_F .

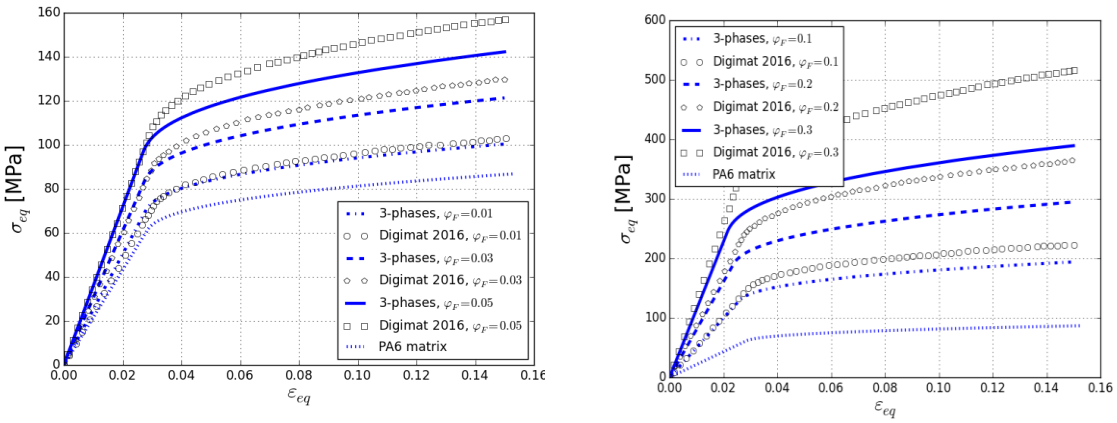

(a) **(b)**

Figure 3: Effective response of 3-phases composite under uniaxial loading: (a) low volume fraction; (b) increasing volume fraction

Figure 4 presents the influence of the imperfection at both scales of the 2-phases and 3-phases composites. The effective response for the 2-phases composite is presented in Figure 4-a. The sliding coefficient α_{01} shows an influence on the stress-strain response. Even the variation seems very weak, the higher the sliding coefficient α_{01}, the weaker the 2-phases composite response. Figure 4-b presents the combined effect of a sliding at both 2-phases and 3-phases composites. The higher α_{02}, the weaker the mechanical response in terms of young modulus, yield stress and hardening modulus.

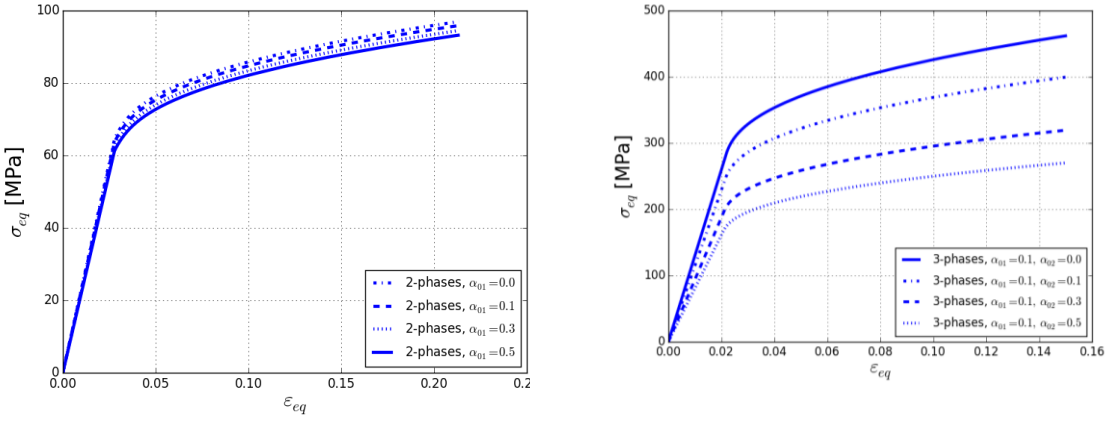

(a) **(b)**

Figure 4: Effect of the imperfection on the response of 2-phases and 3-phases composites: (a) 2-phases composite; (b) 3-phases composite.

Besides, the damage parameter D within the polymer matrix PA6 is studied versus the volume fraction φ_F in Figure 5. Beyond the elastic zone, the volume fraction φ_F has an impact on the damage of the matrix, which increases when φ_F is high. A similar trend is confirmed for the strain energy release $\mathbf{Y}$ of the 3-phases composite as shown by Figure 5-b. The higher the volume fraction φ_F, the higher the strain energy release.

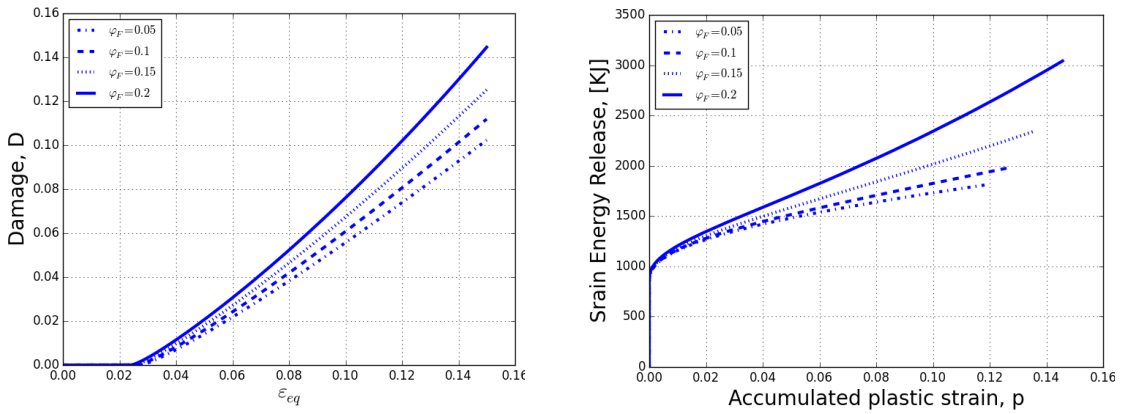

(a) **(b)**

Figure 5: Damage and strain energy release for a perfect interface under uniaxial loading: (a) Damage parameter; (b) Strain energy release

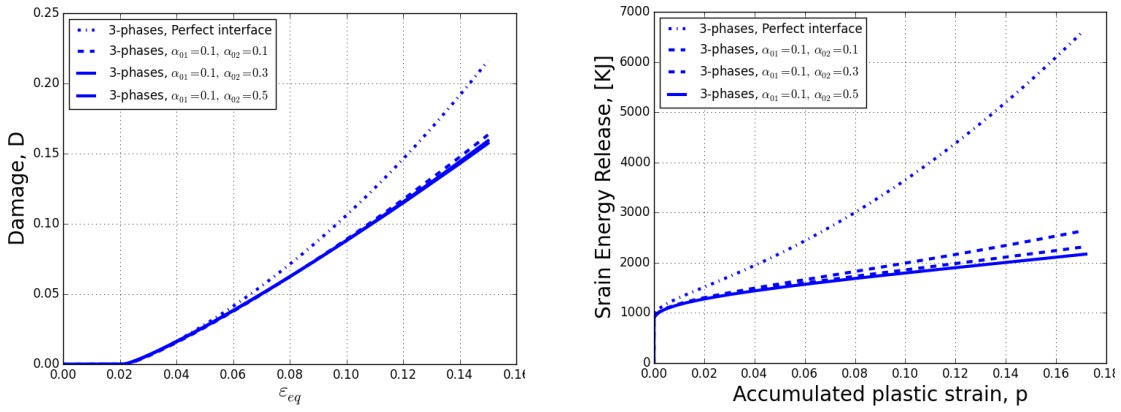

(a) **(b)**

Figure 6: Damage and strain energy release for an imperfect interface under uniaxial loading: (a) Damage parameter; (b) Strain energy release

Figure 6 shows the variation of the damage parameter $\mathbf{D}$ and the strain energy release $\mathbf{Y}$ as a function of the interfacial sliding coefficient. It is seen in Figure 6-a that the damage $\mathbf{D}$ increases highly from the imperfection interface to the configuration of the perfect interface. No significant variation is noticed in the evolution of $\mathbf{D}$ for imperfect interface when α_{02} has increased. The damage $\mathbf{D}$ and the sliding coefficients are the parameters that weaken the material stiffness. We assume no coupling between these parameters, which remain independent variables. Concerning the strain energy $\mathbf{Y}$, a huge difference is noticed between the perfect interface and the imperfect one. In addition, for the imperfect interface, the sliding coefficient α_{02} shows an impact on the strain energy $\mathbf{Y}$, the higher α_{02}, the lower the strain energy $\mathbf{Y}$. In general, the strain energy $\mathbf{Y}$ decreases when the imperfection is growing within the microstructure.

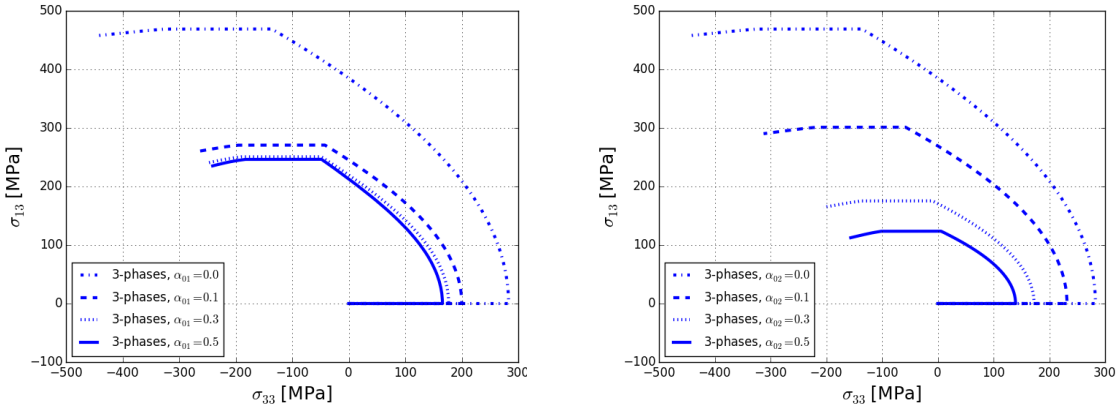

(a) **(b)**

Figure 7: Effective response of 3-phases composite under tension-torsion loading: (a) GNPs/polymer interface α_{01}; (b) Glass fibers/polymer interface α_{02}

Results in Figure 7 have been obtained for a tension-torsion loading. The loading is given by a macro time dependent stain increment $\Delta\mathbf{E}(t)$ such as:

$$\Delta\mathbf{E}(t)=\Delta E_{33}(t)\left[-\frac{1}{2}\mathbf{e}_1\otimes\mathbf{e}_1-\frac{1}{2}\mathbf{e}_2\otimes\mathbf{e}_2+\mathbf{e}_3\otimes\mathbf{e}_3\right]+\Delta E_{13}(t)\left[\mathbf{e}_1\otimes\mathbf{e}_3+\mathbf{e}_3\otimes\mathbf{e}_1+\mathbf{e}_2\otimes\mathbf{e}_3+\mathbf{e}_3\otimes\mathbf{e}_2\right] \quad (17)$$

where the analytical expressions of the axial $\Delta E_{33}(t)$ and shear $\Delta E_{13}(t)$ strain components can be deduced from Figure 2b of works by Lahellec and Suquet [33]. Both interfacial conditions represented by α_{01} for the graphene/polymer interface and α_{02} for the fibers/polymer interface are considered in the analysis. Firstly, .an axial strain $\Delta E_{33}(t)$ is applied with no applied shear. This stage corresponds to a tensile loading. A decrease of the tensile modulus σ_{33} is therefore obtained in Figure 7-a from a perfect interface case $\alpha_{01}=0.0$ to an imperfect case for instance $\alpha_{01}=0.5$ with respect to the GNPs/polymer interface. A similar trend is observed in Figure 7-b for the fibers/polymer interface. Next, a shear deformation $\Delta E_{13}(t)$ is applied while the axial strain $\Delta E_{33}(t)$ is kept constant at its maximum threshold. The modulus σ_{13} increases under this loading condition. Finally, axial strain $\Delta E_{33}(t)$ is decreased to zero while the shear strain $\Delta E_{13}(t)$ is kept constant. For

these last loading condition, a decrease in the composite response is noticed versus the sliding coefficients α_{01} and α_{02}. It appears from a comparison between Figure 7-a and Figure 7-b that below a sliding coefficient value, the fibers/polymer interface is the principal driven mechanism in the degradation of the composite stiffness in the shear direction σ_{13}.

5. Conclusion

The nonlinear effective mechanical properties have been studied during this work, for hybrid fibers reinforced graphene polymer matrix composites. To deal with the material length scale, the modelling strategy is based on mean-field homogenization techniques. Interfacial imperfections mainly the GNPs/Polymer and the fibers/polymer interfaces are considered through a linear spring model LSM. Three phases are involved in the modelling leading to a hierarchical modelling strategy. The volume fraction of the fibers and the sliding coefficient at the interface as well as the aspect ratio are the selected design parameters of the study.

Numerical results, performed on a short Glass fibers reinforced GNPs polymer PA6 matrix, show that the volume fraction and the sliding coefficient greatly influence the effective nonlinear stress-strain behavior. The higher the volume fraction of the fibers, the stiffer the composite. The higher the sliding coefficient, the lower and softer the mechanical response of the composite. On the other hand, it has been seen through a tension torsion loading that the fibers/polymer interface is the most likely parameter to damage the composite mainly under a shear loading. The developed methodology is versatile modeling, which is used analytically in this work. As a perspective, it will be implemented numerically through a user-defined material UMAT for analyzing the multiscale behavior of the 3-phases composites for automotive applications like crashworthiness.

Acknowledgments

This work was supported by the European Union Seventh Framework Programme under grant agreement No. 604391 and Horizon 2020 Programme under grant agreement No. 696656 Graphene Flagship.

Received: ((will be filled in by the editorial staff))
Revised: ((will be filled in by the editorial staff))
Published online: ((will be filled in by the editorial staff))

References

[1] Aldajah S, Haik Y. Transverse strength enhancement of carbon fiber reinforced polymer composites by means of magnetically aligned carbon nanotubes. *Materials & Design*. **2012**; 34: 379 – 383.

[2] E Bekyarova, Thostenson ET, Yu A, Kim H, J Gao, Tang J, et al. Multiscale Carbon Nanotube-Carbon Fiber Reinforcement for Advanced Epoxy Composite. *Langmuir*. **2007**; 23(7):3970–3974.

[3] Jiang S, Li Q, Wang J, He Z, Zhao Y, Kang M. Multiscale graphene oxide-carbon fiber reinforcements for advanced polyurethane composites. *Composites Part A: Applied Science and Manufacturing*. **2016**; 87: 1 – 9.

[4] Yang X, Wang Z, Xu M, Zhao R, Liu X. Dramatic mechanical and thermal increments of thermoplastic composites by multi-scale synergetic reinforcement: Carbon fiber and graphene nanoplatelet. *Materials & Design*. **2013**; 44: 74 – 80.

[5] Ege D, Kamali AR, Boccaccini AR. Graphene Oxide Polymer Based Biomaterials. *Advanced Engineering Materials*. **2017**;19 (12): 1700627.

[6] Huang WM, Sun WF, Chen GH, Tan L. Nanocavities Double the Toughness of Graphene–Polycarbonate Composite. *Advanced Engineering Materials*. **2014**; 17(3): 299–304.

[7] Lu X, Munief WM, Heib F, Schmitt M, Britz A, Grandthyl S, et al. Front End of Line Integration of Graphene Oxide for Graphene Based Electrical Platforms. *Advanced Materials Technologies*. **2018**; 3(4): 1700318.

[8] Rafiee MA, Rafiee J, Srivastava I, Wang Z, Song H, Yu ZZ, et al. Fracture and Fatigue in Graphene Nanocomposites. *Small*. **2010**; 6(2): 179–183.

[9] Veca LM, Meziani MJ, Wang W, Wang X, Lu F, Zhang P, et al. Carbon Nanosheets for Polymeric Nanocomposites with High Thermal Conductivity. *Advanced Materials*. **2009**; 21(20): 2088–2092.

[10] Xu Z, Gao C. In situ Polymerization Approach to Graphene-Reinforced Nylon-6 Composites. *Macromolecules*. **2010**; 43(16): 6716–6723.

[11] Zhang WL, Park BJ, Choi HJ. Colloidal graphene oxide/polyaniline nanocomposite and its electrorheology. *Chem Commun*. **2010**; 46: 5596–5598.

[12] Pedrazzoli D, Pegoretti A, Kalaitzidou K. Synergistic effect of exfoliated graphite nanoplatelets and short glass fiber on the mechanical and interfacial properties of epoxy composites. *Composites Science and Technology*. **2014**; 98: 15 – 21.

[13] Pedrazzoli D, Pegoretti A, Kalaitzidou K. Synergistic effect of graphite nanoplatelets and glass fibers in polypropylene composites. *Journal of Applied Polymer Science*. **2015**; 132(12).

[14] Greco A, Lionetto F, Maffezzoli A. Orientation of Graphene Nanoplatelets in Thermosetting Matrices. *IEEE Transactions on Nanotechnology*. **2016** Nov; 15(6): 877–883.

[15] Mahmood H, Tripathi M, Pugno N, Pegoretti A. Enhancement of interfacial adhesion in glass fiber/epoxy composites by electrophoretic deposition of graphene oxide on glass fibers. *Composites Science and Technology*. **2016**; 126: 149 – 157.

[16] Qingbo Zhang, Dawei Jiang, Li Liu, Yudong Huang, Jun Long, Guangshun Wu, Zijian Wu, Ahmad Umar, Jiang Guo, Xi Zhang, and Zhanhu Guo. Effects of graphene oxide modified sizing agents on interfacial properties of carbon fibers/epoxy composites. J*ournal of Nanoscience and Nanotechnology*. **2015**; 15(12): 9807–9811.

[17] Elmarakbi A, Azoti W, Serry M. Multiscale modelling of hybrid glass fibres reinforced graphene platelets polyamide {PA6} matrix composites for crashworthiness applications. *Applied Materials Today*. **2017**; 6:1 – 8.

[18] Jr LM, Dai G. Hybrid and hierarchical nanoreinforced polymer composites: Computational modelling of structure-properties relationships. *Composite Structures*. **2014**; 117:156 – 168.

[19] Feng C, Wang Y, Kitipornchai S, Yang J. Effects of Reorientation of Graphene Platelets (GPLs) on Young's Modulus of Polymer Nanocomposites under Uni-Axial Stretching. *Polymers*. **2017**; 9(10).

[20] Feng C, Wang Y, Yang J. Effects of Reorientation of Graphene Platelets (GPLs) on Young's Modulus of Polymer Composites under Bi-Axial Stretching. *Nanomaterials*. **2018**; 8(1).

[21] Böhm HJ. Continuum Models for the Thermomechanical Behavior of Discontinuously Reinforced Materials. *Advanced Engineering Materials*. **2004**; 6(8):626–633.

[22] Azoti W, Elmarakbi A. Constitutive modelling of ductile damage matrix reinforced by platelets-like particles with imperfect interfaces: Application to graphene polymer nanocomposite materials. *Composites Part B: Engineering*. **2017**; 113:55 – 64.

[23] Azoti WL, Elmarakbi A. Micromechanics Modelling of Graphene Platelets Reinforced Polymer Composite Materials With Imperfect Interfaces. *ASME International Mechanical Engineering Congress and Exposition*. **2016**; 12(50664):1–9.

[24] Azoti WL, Elmarakbi A. Multiscale modelling of graphene platelets-based nanocomposite materials. *Composite Structures***. 2017***;* 168: 313 – 321.

[25] Qu J. The effect of slightly weakened interfaces on the overall elastic properties of composite materials. *Mechanics of Materials*. **1993**; 14(4): 269 – 281.

[26] Qu J. Eshelby Tensor for an Elastic Inclusion With Slightly Weakened Interface. *Journal of Applied Mechanics*. **1993**; 60(4): 1048–1050.

[27] Eshelby JD. The Determination of the Elastic Field of an Ellipsoidal Inclusion, and Related Problems. *Proceedings of the Royal Society of London Series A, Mathematical and Physical Sciences*. **1957**; 241(1226):376–396.

[28] Doghri I, Ouaar A. Homogenization of two-phase elasto-plastic composite materials and structures: Study of tangent operators, cyclic plasticity and numerical algorithms. *International Journal of Solids and Structures*. **2003**; 40(7):1681 – 1712.

[29] Azoti WL, Tchalla A, Koutsawa Y, Makradi A, Rauchs G, Belouettar S, et al. Mean-field constitutive modeling of elasto-plastic composites using two (2) incremental formulations. *Composite Structures*. **2013**; 105: 256–262.

[30] Cho J, Luo JJ, Daniel IM. Mechanical characterization of graphite/epoxy nanocomposites by multi-scale analysis. *Composites Science and Technology*. **2007**; 67(1112): 2399 – 2407.

[31] Xiao JR, Gama BA, Jr JWG. An analytical molecular structural mechanics model for the mechanical properties of carbon nanotubes. *International Journal of Solids and Structures*. **2005**; 42: 3075 – 3092.

[32] Company MS. Digimat User's Manual, E-xstream Engineering; **2016**.

[33] Lahellec N, Suquet P. Effective response and field statistics in elasto-plastic and elasto-viscoplastic composites under radial and non-radial loadings. *International Journal of Plasticity*. **2013**; 42: 1 – 30.